# Role of advanced soil modelling in the dynamic analysis of offshore wind turbines

# Rôle des modèles de sol avancés dans l'analyse dynamique des éoliennes en mer

Federico Pisanò
*Department of Geoscience and Engineering, Delft University of Technology, The Netherlands, F.Pisano@tudelft.nl*

Simone Corciulo, Omar Zanoli
*Marine & Offshore Engineering, D'Appolonia S.p.A., Italy*

ABSTRACT: The increasing relevance of offshore wind in the energy mix motivates continual research efforts for the optimisation of foundation systems. Currently, monopiles are still the most common foundations for offshore wind turbines (OWTs), due to their simplicity and the low costs for production/assembly. However, the modern trends towards larger OWTs and water depths pose new geotechnical challenges in the design of more cumbersome and expensive monopiles. In this work, the potential of 3D finite element (FE) modelling for OWT applications is illustrated. The dynamic response of a soil-monopile-OWT system is numerically simulated by accounting for (i) dynamic hydro-mechanical (HM) coupling in the soil and (ii) cyclic plasticity modelling. In particular, the UCSD08 sand model developed by Yang and Elgamal (2008) has been adopted and calibrated against laboratory test results on medium dense sand. FE results are presented to highlight the combined influence of wind/wave loading and soil non-linearity on the dynamic OWT performance (and specifically on the main natural frequency). The results presented support the beneficial role that 3D FE modelling may play in the improvement of existing design methods.

RÉSUMÉ : La pertinence croissante de l'éolien en mer dans le mix énergétique stimule en continu les efforts de recherche portants sur l'optimisation des systèmes de fondation. A ce jour, les monopieux restent la solution de fondation la plus répandue pour les éoliennes en mer (EEM) de par leur simplicité et les faibles coûts de production/assemblage. La tendance actuelle à des EEM plus imposantes et à de plus grandes profondeurs pose cependant des défis nouveaux quant au dimensionnement de monopieux plus lourds et plus chers. Dans ce présent travail, le potentiel des modèles 3D par éléments finis (EF) pour des applications impliquant des éoliennes en mer est illustré. La réponse dynamique d'un système sol-monopieu-éolienne est simulée en intégrant (i) un couplage dynamique hydromécanique du sol ainsi que (ii) un comportement de plasticité cyclique. En particulier, le modèle de sable UCSD08 mis-au-point par Yang et Elgamal (2008) a été adopté et calibré par des essais en laboratoire sur un sable moyennement dense. Les résultats obtenus par EF sont présentés pour souligner l'influence combinée des efforts du vent/ de la houle et de la non-linéarité du sol sur la performance dynamique des EEM (et spécifiquement sur la fréquence propre principale). Les résultats appuient le rôle bénéfique que la modélisation par EF-3D peut jouer dans l'amélioration des méthodes de dimensionnement.

KEYWORDS: offshore wind turbine, monopile, sand, cyclic plasticity modelling, hydro-mechanical coupling, dynamic analysis

## 1 INTRODUCTION

Since the late 1990s, the production of wind energy has started to move offshore in the North Sea, Baltic Sea and Irish Sea, where high exposure to wind ensures large power productions (Figure 1). According to the European Wind Energy Association (EWEA), Europe currently leads the offshore wind industry with a total offshore power capacity of 8GW in 2014, to become 24GW by 2020 and 66.5GW by 2030 (Gazzo et al. 2015). Massive developments are also expected outside of Europe: Asia is targeting 35GW of offshore installations by 2020, starting from 480MW in 2014. Interesting possibilities for further expansion in the Pacific and the Indian Oceans are also envisaged.

Figure 1. Egmond aan Zee Offshore Wind Farm (Netherlands).

At present, most OWTs are supported by monopile foundations, open-ended steel tubes driven into the seabed through hydraulic hammering. Monopile design can largely affect OWT dynamics, especially the natural frequency $f_0$ associated with the first cantilever-like eigenmode. Accurate estimation of $f_0$ is extremely important to prevent undesired resonance under the vibration induced by wind/wave loads and blade rotation.

This works responds to the need for fundamental research in offshore wind sciences recently remarked by the European Academy of Wind Energy (EAWE). As for geotechnical issues, van Kuik et al. (2016) pointed out two important research questions: "*what is the amount of soil damping for an offshore turbine? Is it possible to estimate soil damping from first principles, like from numerical simulation with solid elements?*". Taking the EAWE agenda as a reference, it is shown hereafter how non-linear 3D FE modelling can enhance the analysis of OWTs and the understanding of related geotechnical aspects (Cuellar et al. 2014; Corciulo et al. 2016). For this purpose, the OpenSees simulation platform (Mazzoni et al. 2007) and advanced soil modelling are exploited to capture the interplay of cyclic effects and HM coupling under environmental loading.

## 2 REFERENCE OWT AND ENVIRONMENTAL LOADS

### 2 .1 *Structural set-up*

All results presented in the following concern a typical 5MW OWT as defined by Jonkman et al. (2009). Figure 2 depicts the reference problem under consideration: the monopile is wished-

in-place into the soil, while the turbine is modelled as a 1D Timoshenko beam subjected to wind/wave thrust forces ($F_{wind}$ and $F_{wave}$). In addition to the distributed mass of the beam, the model includes the mass ($M$) with rotational inertia ($I_M$) of the OWT hub, as well as the added mass ($m_w$) of the surrounding sea water. All structural specifications are listed in Table 1.

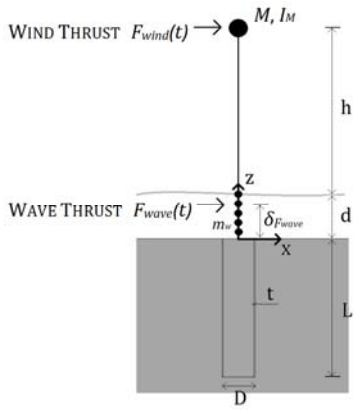


Figure 2. Reference 5MW OWT under wind/wave loading.

Table 1. Structural properties of the OWT-monopile system.

| $h$ [m] | $d$ [m] | $L$ [m] | $D$ [m] | $t$ [cm] | $M$ [tons] | $I_M$ [tons·m$^2$] | $m_w$ [tons] |
|---|---|---|---|---|---|---|---|
| 90 | 20 | 20 | 5 | 5 | 350 | 2600 | 785 |

### 2 .2 *Wind and wave loading*

The loading time histories in Figures 3 and 4 are defined to analyse the transient performance of the reference OWT. Relatively short duration (30 s) are considered in all cases to alleviate the computational costs of 3D FE computations. Four $F_{wind}$ and $F_{wave}$ scenarios (A, B, C, D) are set to represent four average wind speeds, namely 5, 10, 15, 20 m/s:

i. $F_{wind}$ time histories are obtained by converting anemometric records from the Irish Sea through the Blade Element Momentum (BEM) theory (Lanzafame and Messina, 2007);
ii. $F_{wave}$ time histories are derived for a mono-harmonic sea state via the spectrum equation proposed Pierson and Moskowitz (1964). The conversion from wave spectra to thrust forces is performed via the well-known Morison equation (Vugts et al. 2001). It should be noted that wave amplitude and period increase at larger wind speed.

$F_{wind}$ and $F_{wave}$ are gradually applied through 5 s ramps to avoid failure of FE simulations due to sudden load application.

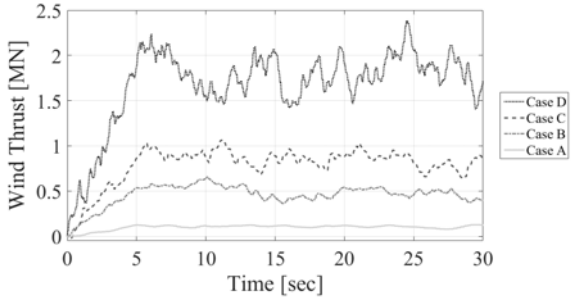


Figure 3. Wind thrust time histories.

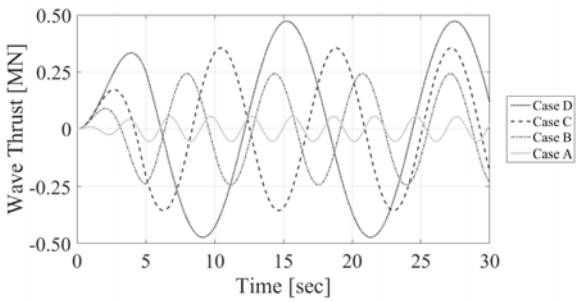


Figure 4. Wave thrust time histories.

## 3 SOIL-MONOPILE 3D FE MODELLING

### 3 .1 *Governing equations and FE solution*

The monopile is assumed to interact with a homogenous sand deposit, whose dynamic HM response is described by means of the well-known *u-p* formulation. This relies upon the assumption of negligible soil-fluid relative acceleration, which suits offshore applications as well as earthquake engineering problems.

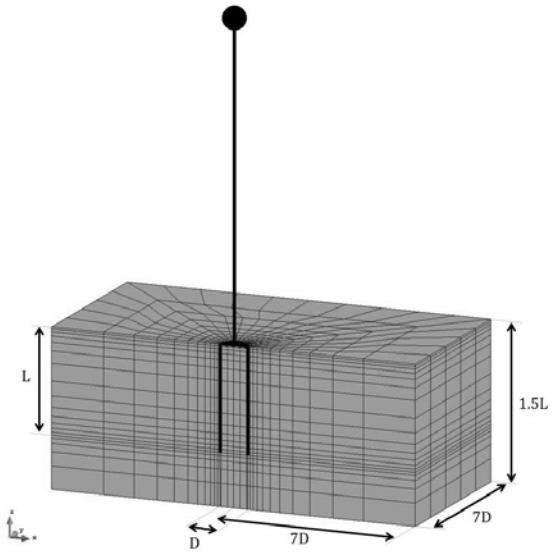


Figure 5. SSP FE discretization of the soil domain.

The soil domain in Figure 5 is discretized with approximately 6000 8-node bricks of the SSP type proposed by McGann et al. (2015). Two-phase SSP elements feature a stabilised equal-order formulation to avoid spurious pore pressure oscillations close to the undrained-incompressible limit. At variance with the OWT beam, the steel monopile is modelled by means of one-phase SSP solid elements.

After space discretization, discrete *u-p* equations are integrated in time through the implicit Newmark algorithm ($\Delta t$= 0.004 s, $\beta$=0.25, $\gamma$=0.5) in combination with explicit forward Euler integration of soil constitutive equations.

### 3 .2 *Calibration of the UCSD08 sand model*

Cyclic sand behaviour is simulated through the UCSD08 multi-surface elasto-plastic model (Yang and Elgamal 2008), capable of reproducing cyclic hysteresis and undrained cyclic mobility under shear loading. Unlike other cyclic models, the UCSD08 formulation is not sensitive to variations in void ratio and cannot reproduce sand densification around the monopile (LeBlanc et al. 2010). However, densification effects are not

deemed too relevant when the transient OWT response is analysed over relatively short loading events.

Figure 6 shows the good UCSD08 simulation of a cyclic triaxial test on a medium dense sand specimen ($D_R$~60%) from offshore Myanmar (left: *q-p'* stress path; right: pore pressure vs time). The sand parameters calibrated and used throughout this work are reported in Table 2. A permeability $k$=5·10$^{-4}$ m/s has been also estimated.

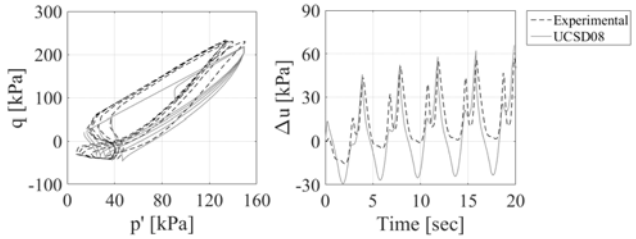


Figure 6. UCSD08 simulation a cyclic two-way triaxial test (initial effective stresses $\sigma'_{0v}$=187 kPa and $\sigma'_{0h}$=90 kPa).

Table 2. UCSD08 parameters for the sand considered in this study.

| $G_r$ [kPa] | $K_r$ [kPa] | $p'_r$ [kPa] | $n$ [-] | $\Phi'$ [deg] | $\gamma_{max}$ [%] | $\Phi_{PT}$ [deg] | $\rho$ [tons/m$^3$] |
|---|---|---|---|---|---|---|---|
| 1×10$^5$ | 1.7×10$^5$ | 100 | 0.5 | 35.5 | 8.5 | 31 | 1.8 |
| $c_1$ [-] | $c_2$ [-] | $c_3$ [-] | $d_1$ [-] | $d_2$ [-] | $d_3$ [-] | $p'_y$ [-] | $\gamma s_{max}$ [%] |
| 0.125 | 0.5 | 1 | 0.25 | 3.9 | 5.7 | 1.95 | 0.0 |

## 4 SOIL-MONOPILE-OWT DYNAMIC PERFORMANCE

The soil-monopile-OWT dynamic response to the four loading scenarios in Section 2.2 is described in what follows.

### 4 .1 *Soil-monopile interaction*

Figure 7 exemplifies the cyclic response at a shallow soil location for the loading scenario C (average wind speed: 15 m/s); the colorbar on the side represents time elapsing over the interval 0-30 s. Plots clearly depict the main features of the cyclic HM response of the medium dense sand:

i. the stress-strain response exhibits pronounced non-linearity under shear loading, including hysteretic dissipation loops and strain accumulation;
ii. as the soil tends to dilate above the phase transformation line, negative pore pressure increments are generated, along with increases in mean effective stress $p'$ and, as a consequence, soil strengthening/stiffening.

Point (ii) is a typical outcome of deviatoric/volumetric coupling in soils, becoming very relevant when substantial soil non-linearity is mobilised (e.g. under storm conditions). Such a feature is hardly captured by simpler constitutive modelling.

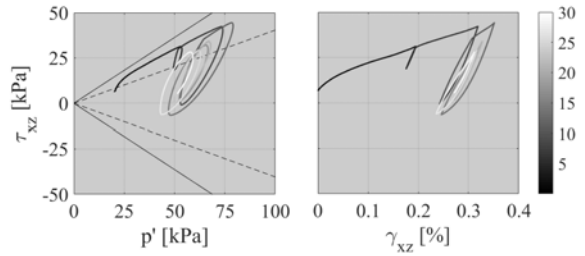


Figure 7. Soil shear stress-strain response and effective stress path 4 m right of the monopile and 3.6 m below the mudline (scenario C).

The integral of all local responses within the soil domain determines the global performance of the foundation. Figure 8 illustrates the horizontal load-displacement responses at the monopile head under the cyclic loading histories A, B, C, D.

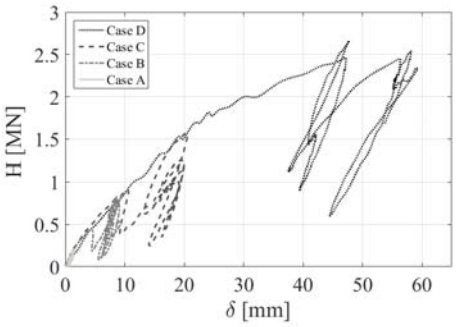


Figure 8. Horizontal load-displacement responses at the monopile head.

Although the four loading scenarios feature different numbers of wave cycles (the total duration is 30 s in all cases), Figure 8 suggests some relevant observations:

1. expectedly, all curves share the same virgin backbone branch, describing the response to $F_{wind}$ rising from 0 to the final average value (Figure 3);
2. during cyclic loading, increasing amount of energy is dissipated through unloading/reloading hysteresis at larger loading amplitude;
3. the average unloading/reloading stiffness depends on the loading amplitude, and is not straightforward to identify in presence of progressive displacement accumulation.

The third finding stems from the fact that, even during unloading/reloading cycles, soil plastifications occur around the monopile. The extent of plastic straining throughout the soil domain depends on the loading amplitude and determines the evolution of the dynamic monopile stiffness. The lateral stiffness of the monopile head affects the OWT dynamics along with the moment-rotation response – not reported for brevity.

### 4 .2 *OWT dynamics*

Figure 9 reports the simulated displacements $\delta$ of the OWT hub under the wind/wave load combinations A, B, C, D. The results are compared to the predictions obtained for a OWT clamped at the mudline (lighter lines) and emphasize the influence of the foundation compliance. The variations in wind/wave thrusts are not only responsible for different vibration amplitudes, but also affect the dominant oscillation period through soil non-linearity.

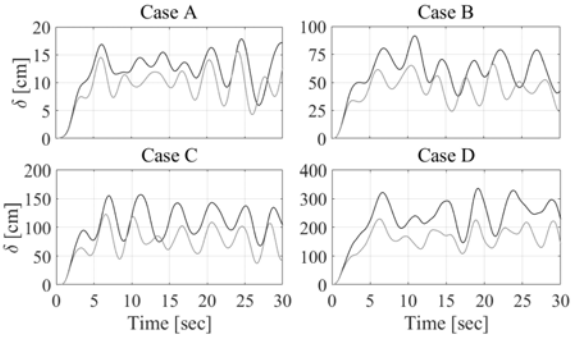


Figure 9. Displacement time histories at the OWT hub.

The same results in Figure 9 are also visualised in the frequency domain in terms of normalised[1] power spectral density (PSD):

$$PSD(f) = \left|\hat{\delta}(f)\right|^2 \quad (1)$$

derived from the Fourier transform of the hub displacement $\delta$ (Figure 10). Natural frequencies $f_0$ correspond with the highest PSD peaks – also compared to the $f_0$ value obtained for the clamped turbine (vertical dashed line).

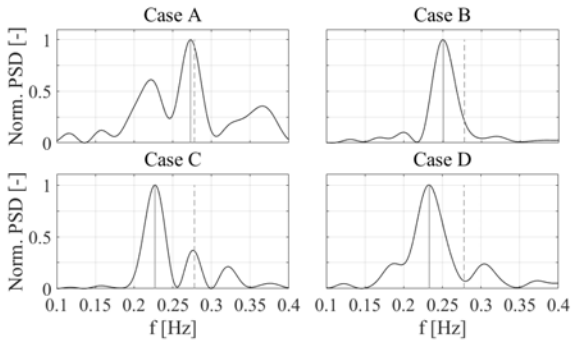


Figure 10. Displacement power spectral densities at the OWT hub.

$f_0$ is affected by the interaction between loading amplitude and geotechnical factors. In particular, the following statements apply to the shear stiffness of dilative sands:

i. stiffness increases at larger effective confinement $p'$;
ii. stiffness decreases under shear straining;
iii. volume HM effects result in higher stiffness.

As summarised in Table 3, the decrease in $f_0$ at increasing wind speed is not strictly monotonic, with a slight increase in $f_0$ recorded at the transition from 15 to 20 m/s. This interesting finding seems related to the peculiar evolution of the lateral monopile stiffness (Figure 8), and could not be detected by traditional analyses based on *p-y* modelling (Doherty and Gavin 2012).

Table 3. $f_0$ values computed for the loading scenarios A, B, C, D.

| | *Case A* | *Case B* | *Case C* | *Case D* |
|---|---|---|---|---|
| $f_0$ [Hz] | 0.270 | 0.251 | 0.227 | 0.233 |

## 5 CONCLUDING REMARKS

A 3D HM FE model was developed to analyse a standard 5 MW OWT founded on a monopile in a homogeneous sand deposit. Four wind/wave loading scenarios were considered to explore the effects of wind speeds in the range from 5 to 20 m/s. Advanced FE modelling was exploited to account at the same time for slow soil dynamics, pore pressure effects and non-linear cyclic soil behaviour.

The FE results put in evidence some interesting aspects about the interplay of loading amplitude and soil non-linearity. In particular, it was shown that mobilising increasing soil plasticity does not necessarily imply a monotonic decrease in natural frequency, also as a consequence of lesser investigated dilatancy effects.

Future work along this research line will be devoted to investigate the response of soil-monopile-OWT systems in combination with different soil stratigraphies and monopile sizes. In this context, parallel computing will be essential to simulate longer loading histories and support the refinement of existing design methods.

[1] PSDs are normalised by their maximum value, implying 0≤PSD≤1.

## 6 ACKNOWLEDGEMENTS

D'Appolonia S.p.A (San Donato Milanese, Italy) and Siemens Wind Power (The Hague, The Netherlands) are gratefully acknowledged for providing soil data and anemometric records, respectively.

## 7 REFERENCES

Corciulo S., Zanoli O., Pisanò F. 2016. Transient response of offshore wind turbines on monopiles in sand: role of cyclic hydro-mechanical soil behaviour. *Computers and Geotechnics*, published online, DOI: 10.1016/j.compgeo.2016.11.010.

Cuéllar P., Mira P., Pastor M., Merodo J.A.F., Baeßler M. and Rücker W. 2014. A numerical model for the transient analysis of offshore foundations under cyclic loading. *Computers and Geotechnics*, 59, 75-86.

Doherty P. and Gavin K. 2012. Laterally loaded monopile design for offshore wind farms. In *Proceedings of the Institution of Civil Engineers – Energy*, 165 (1), 7-17.

Gazzo A., Matzen F., Farhangi C. and Lamdaouar, A. 2015. Offshore wind in Europe – Walking the tightrope to success. Technical report, Ernst & Young. London, UK.

Jonkman J.M., Butterfield S., Musial W. and Scott G. 2009. Definition of a 5-MW Reference Wind Turbine for offshore system development. Technical report, National Renewable Energy Laboratory (NREL). Golden, Colorado, USA.

van Kuik G.A.M., Peinke J. Nijssen R., Lekou D.J., Mann J., Sørensen J.N., Ferreira C., van Wingerden J.W., Schlipf D., Gebraad P. et al. 2016. Long-term research challenges in wind energy – a research agenda by the European Academy of Wind Energy. *Wind Energy Science*, 1, 1-39.

Lanzafame R. and Messina M. 2007. Fluid dynamics wind turbine design: critical analysis, optimization and application of BEM theory. *Renewable energy*, 32, 2291-2305.

LeBlanc C., Houlsby G.T. and Byrne B.W. 2010. Response of stiff piles in sand to long-term cyclic lateral loading. *Géotechnique*, 60 (2), 79-90.

Mazzoni S., McKenna F., Scott M. and Fenves G. 2007. *OpenSees Command Language Manual.*

McGann C.R., Arduino P. and Mackenzie-Helnwein P. 2015. A stabilized single-point finite element formulation for three-dimensional dynamic analysis of saturated soils. *Computers and Geotechnics*, 66, 126-141.

Pierson W.J. and Moskowitz L. 1964. A proposed spectral formulation for fully developed wind seas based on the similarity theory of S.A. Kitaigorodskii. *Journal of Geophysical Research*, 69 (24), 5181-5190.

Vugts J.H., van der Tempel J. and Schrama E.A. 2001. Hydrodynamic loading on monotower support structures for preliminary design. In *Proceedings of Offshore Wind Energy EWEA Special Topic Conference. Brussels, Belgium.*

Yang Z. and Elgamal, A. 2008. Multi-surface cyclic plasticity sand model with Lode angle effect. *Geotechnical and Geological Engineering*, 26 (3), 335-348.